AD-A125 199 AN INVESTIGATION OF THE STRUCTURE AND HIGH TEMPERATURE MECHANICAL PROPERT..(U) STANFORD UNIV CA DEPT OF MATERIALS SCIENCE AND ENGINEERING W D NIX DEC 82 1/1

UNCLASSIFIED AFOSR-TR-82-1084 AFOSR-81-0022 F/G 11/6 NL

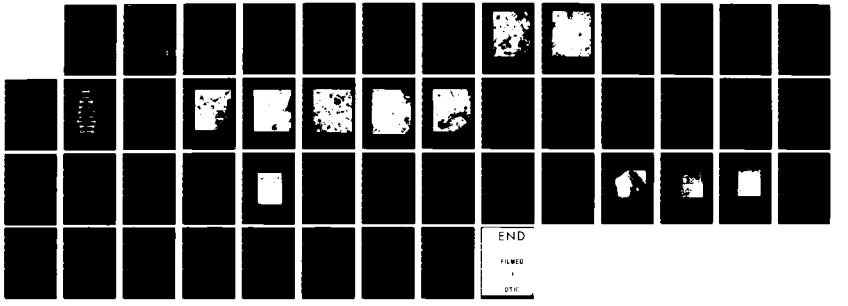

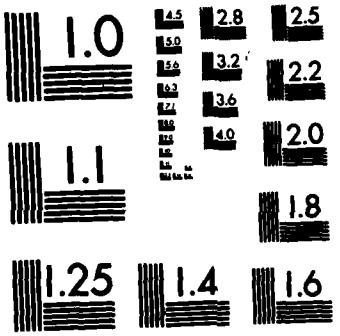

(2)

INTERIM SCIENTIFIC REPORT

(For the period 1 October 1981 to 30 September 1982

(AFOSR GRANT NO. 81 - 0022)

AN INVESTIGATION OF THE STRUCTURE AND HIGH TEMPERATURE MECHANICAL PROPERTIES OF OXIDE DISPERSION STRENGTHENED ALLOYS

Submitted to

Department of the Air Force

Directorate of Electronic and Solid State Sciences

Air Force Office of Scientific Research

Bolling AFB, Building 410, Washington, D.C. 20332

Attn: Dr. Alan H. Rosenstein

Submitted by

Professor William D. Nix (Principal Investigator)

Department of Materials Science and Engineering

Stanford University, Stanford, California 94305

December, 1982

This research was supported by the Air Force Office of Scientific Research (AFSC) under Grant No. AFOSR 81 - 0022

Approved for public release; distribution unlimited

Qualified requestors may obtain additional copies from the Defense Documentation Center; all others should apply to the Clearing House for Federal Scientific and Technical Information

Approved for public release;

TABLE OF CONTENTS

I. SUMMARY OF RESEARCH

The overall objective of this research has been to develop a better understanding of the structure and high temperature mechanical properties of oxide dispersion strengthened metals. In this report we describe the progress we have made during the past year.

Much of our attention during the past year has been focused on the deformation of fine grained ODS nickel based alloys (MA 754 and MA 6000). We have obtained these materials in the as-hot worked condition (rather than the recrystallized condition). This has allowed us to study the deformation properties in the fine grain regime. The alloys MA 754 and MA 6000 have grain sizes of 0.3 μm and 0.7 μm, respectively, in the as-hot worked condition. These materials exhibit remarkable tensile properties in the temperature range 900-1100 C. In particular we find that they exhibit superplastic properties. Unlike ordinary coarse grained ODS alloys, these materials exhibit very high strain rate sensitivities, especially at high strain rates and this naturally leads to high ductilities in tension. For MA 6000 we find the optimum strain rate for superplastic deformation to be about 0.5 s^{-1}. We believe these properties might allow superplastic forming methods to be used to make complex shapes with these alloys.

We have studied the microstructures of these alloys using TEM techniques. Significant grain coarsening occurs at the high temperatures and lower strain rates. However, the grain sizes are still in the 1 μm range even after this coarsening has occurred. There is evidence that recrystallization occurs in MA 754 as a result of deformation but it does not lead to very large grains. It seems likely that sufficient energy can be left in the microstructure

after superplastic deformation to trigger the necessary grain coarsening transformation.

A model has been developed to describe and explain the unusual flow properties of fine grained ODS alloys. It is based on the idea that steady state flow involves the coupling of diffusional and dislocation creep processes. Each of these processes, in turn, operates only if the stress is above a threshold value. We think that oxide particles can inhibit both the glide of crystal dislocations (the Orowan process) and the climb of grain boundary dislocations (the Ashby process). We are currently using this model to understand the superplastic flow properties of ODS alloys. Also, we are testing the predictions of the model by measuring the creep properties at low stresses.

We are continuing our work on the high temperature creep and fracture properties of coarse grained MA 754. During the past year we have extended our creep experiments from 1000 to 1300 C, with most of the new data being obtained at 1200 C. Recent contact with Dr. J. Benjamin of INCO indicates considerable interest in the creep properties of this material at 1200 C and higher. By testing at these high temperatures we have found a new regime of deformation that seems to be strongly affected by cavitation. At high temperatures and low stresses the power law exponent for creep is about 8, whereas at lower temperatures and higher stresses, it is about 35. In addition, the mode of fracture is different in these two regimes. At high stresses fracture occurs transgranularly whereas at low stresses it occurs intergranularly. This strongly suggests that grain boundary cavitation contributes significantly to the creep rate.

We have recently observed particle free zones near grain boundary cavities after creep. These observations strongly suggest a diffusive mechanism for the degradation of transverse grain boundaries under creep conditions. Apparently cavities form at particles on grain boundaries and then grow by diffusional processes. This leads to a plating of matrix material on the grain boundary and the formation of a particle free zone. This in turn weakens the structure severely and leads to failure.

Our work on the structure and high temperature mechanical properties of Al-Fe-Ce alloys is just now getting started. The delay in starting this work has been caused by difficulties associated with obtaining experimental materials. These problems have now been resolved and the work is under way.

II. RESEARCH REPORT

A. Deformation of Fine Grained MA 754 and MA 6000

The deformation behavior of fine grained MA 754 and MA 6000 has been characterized over the range of strain rates from $2x10^{-4}s^{-1}$ to $5\ s^{-1}$ at 900,1000, and 1100 C. This information will ultimately be used to determine the dependence of abnormal grain growth during annealing on prior working history. The microstructures of as-hot worked MA 754 and MA 6000 are shown in Figs. 1 and 2, respectively. For all micrographs, the arrows indicate the direction parallel to the working direction. While both alloys are extremely fine grained, some differences are clear. First, the average grain diameter of the MA 754 sample is larger than that of the MA 6000, 0.67 μm as opposed to 0.26 μm. Second, the grain boundaries in MA 754 are more curved, and less angular than in the MA 6000. Third, despite the kinematic diffracting conditions, the MA 754 reveals a very high dislocation density compared to the MA 6000. Fourth, twins can be readily observed in MA 6000 (only one is evident in Fig. 2), but are not seen in MA 754. Last, no preferred crystallographic orientation is noticeable for the MA 6000, while the MA 754 shows a tendency for [200] to be parallel to the working direction.

The flow stresses of these materials are shown at different strain rates and temperatures in Figs. 3 and 4. The logarithm of the strain rate is plotted against the logarithm of the flow stress for both alloys at all three temperatures. The curves for MA 754 are relatively smooth, but do not show stress exponents of less than 2.5 . Additionally, the curve for MA 754 at 1100 C shows an apparent threshold stress. The curves for MA 6000 have some intriguing features. At 900 and 1000 C, there seems to be a threshold stress. However, at a stress of approximately 100 MPa, the stress exponent

Fig. 1. Microstructure of as-received (as-hot worked) MA 754 as revealed by bright field TEM; the arrow indicates the working direction.

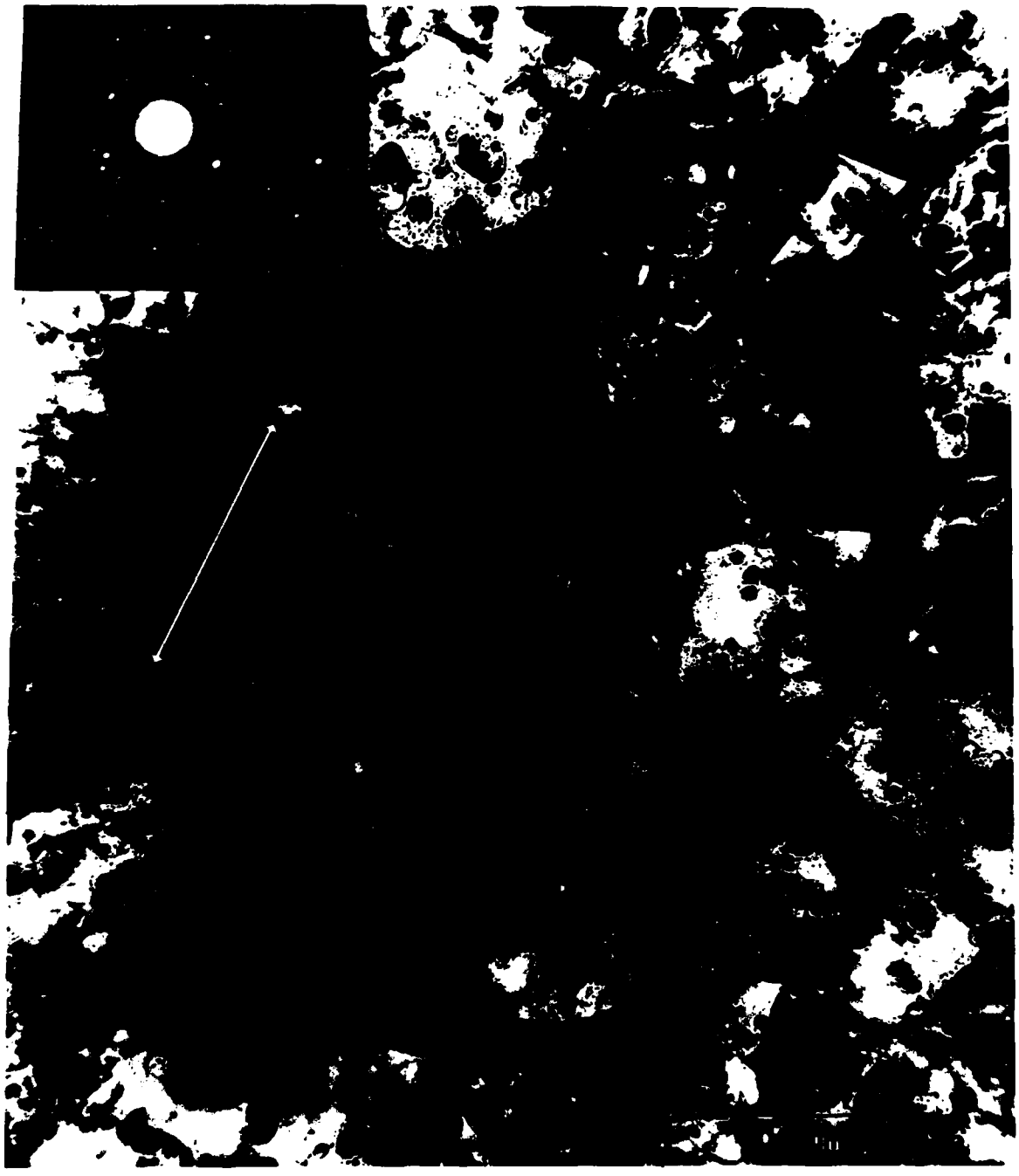

Fig. 2. Microstructure of as-received (as-hot worked) MA 6000 as revealed by bright field TEM. The arrow indicates the working direction.

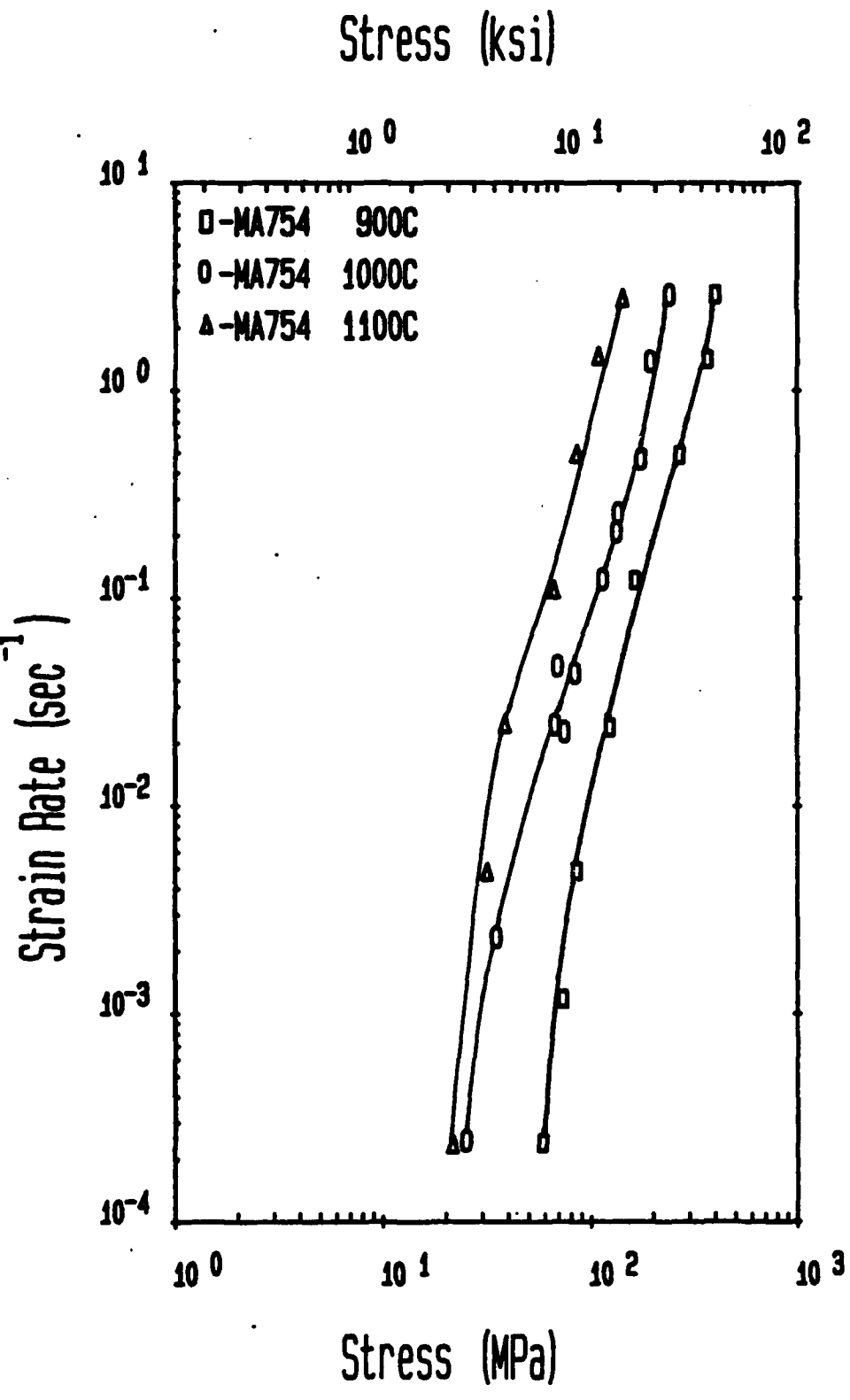

Fig. 3. Steady state flow properties of MA 754 at three different temperatures.

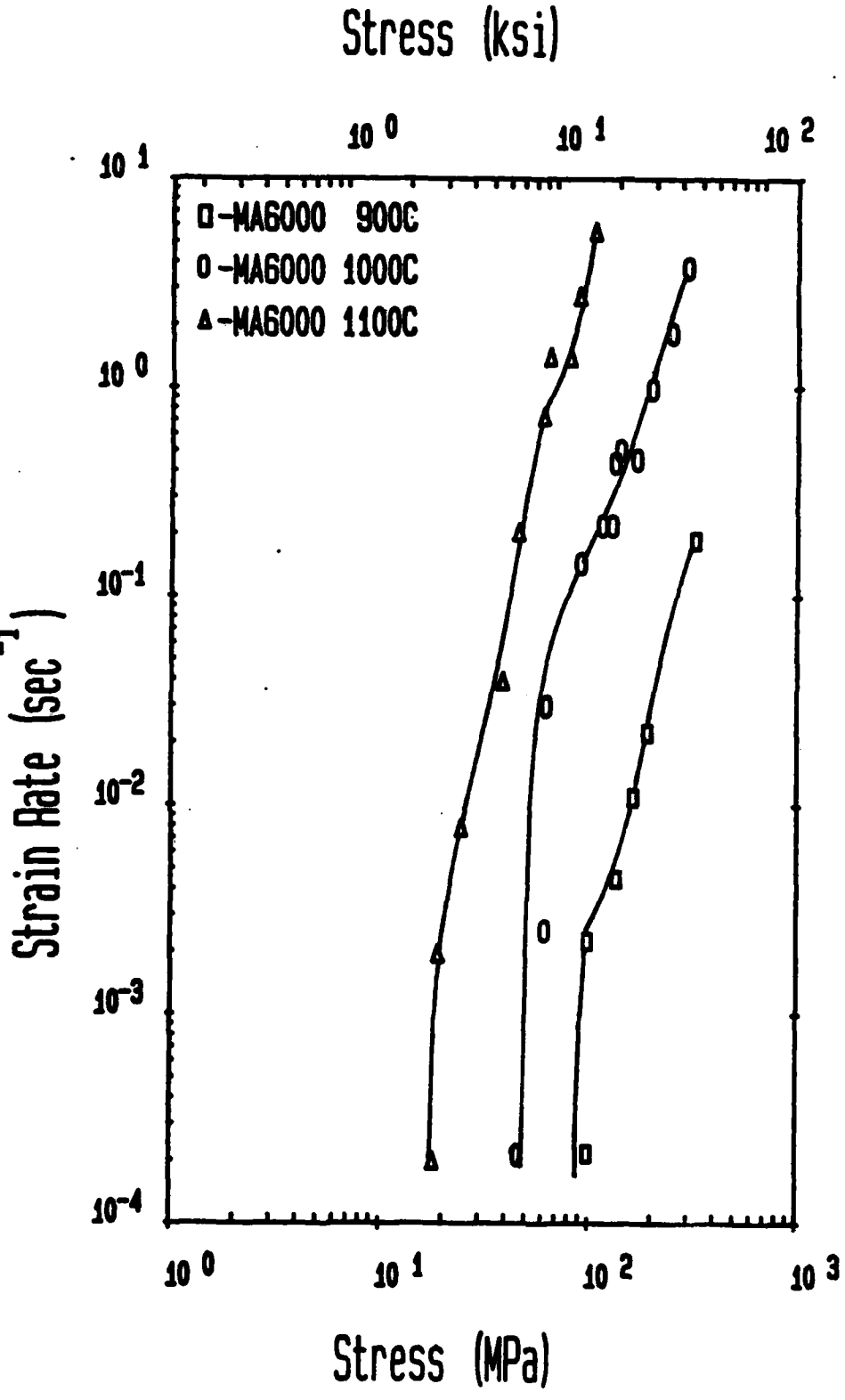

Fig. 4. Steady state flow properties of MA 6000 at three different temperatures.

changes dramatically. The curve for MA 6000 deformed at 1100 C shows a smoother transition from the threshold stress at low strain rates to the low stress exponent regime at high strain rates. Strain rate sensitivities have been obtained by measuring the inverse of the slopes of the curves in Figs. 3 and 4.

While the generally accepted method for measuring the strain rate sensitivity involves cycling between two strain rates and observing the load changes, such testing was ruled out by the high strain rates required to test these extraordinarily fine grained materials. Figure 5 shows an example of a load-time plot from the fastest test, and indicates that the test only lasted a quarter of a second. Although not all tests were this short, those which were of interest were generally less than one minute, which does not allow for repeated strain rate cycling.

An example of a plot of strain rate sensitivity versus strain rate, as well as elongation to failure and reduction in area versus strain rate is given in Fig. 6 for MA 6000 tested at 1000 C. There is a clear correlation between the maximum in strain rate sensitivity and the maximum elongation, although the maximum elongation seems to be offset to higher strain rates. This is undoubtedly due to the fact that the m-values are derived from information taken from the beginning of the test, while the total elongation occurred over the entire time of the test. Since constant crosshead speeds were used, the overall true strain rate continually decreased, so that it is better to associate elongations with somewhat lower strain rates.

The appearance of the specimens which correspond to these data are shown in Fig. 7. Note that gradual necking occurs at intermediate strain rates, but not at very slow or very fast strain rates. Failure at low

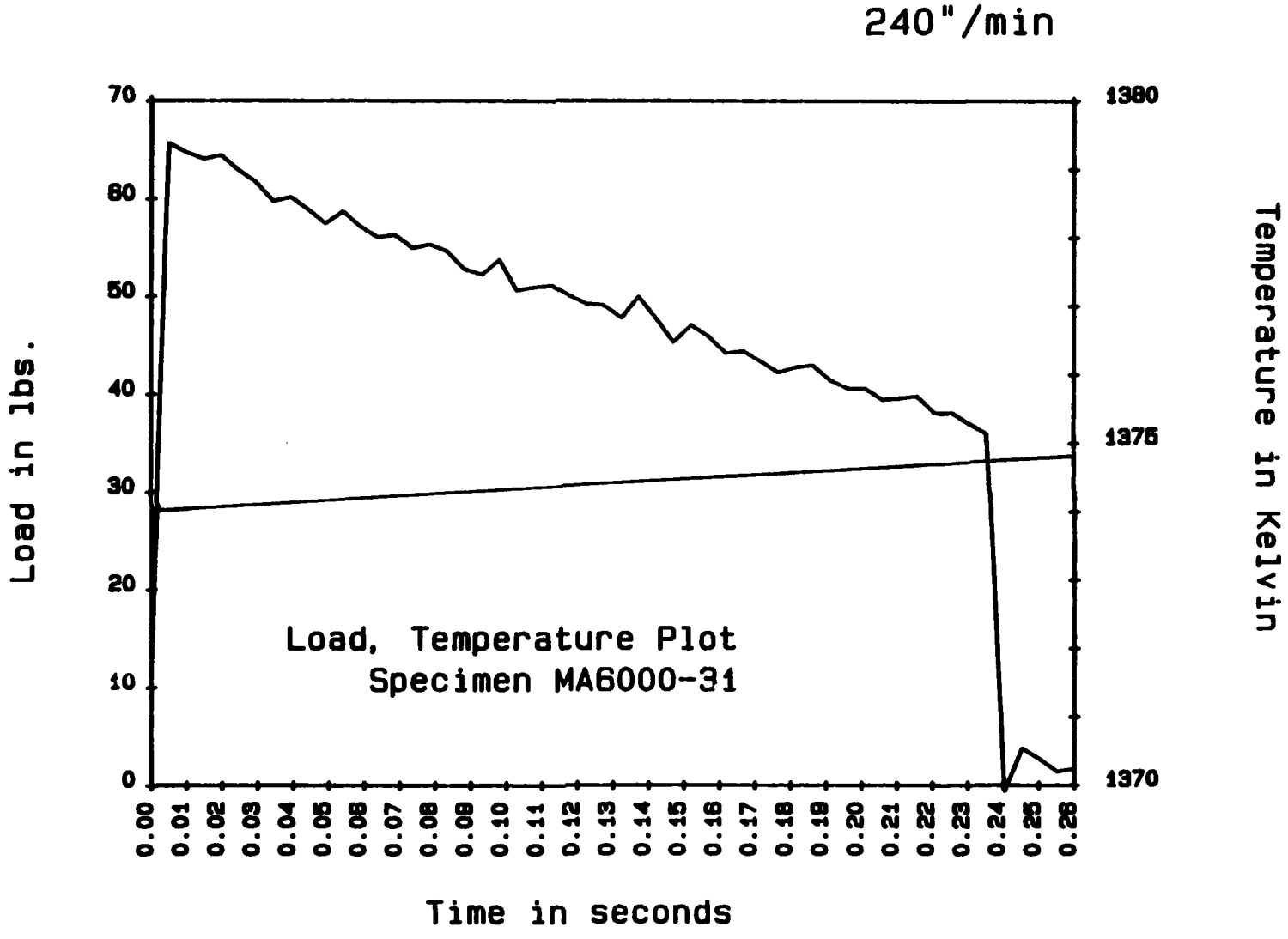

Fig. 5. Load-time response for a fast tensile test conducted on MA 6000 at 1375 K. The extension rate was 240 inch/min !

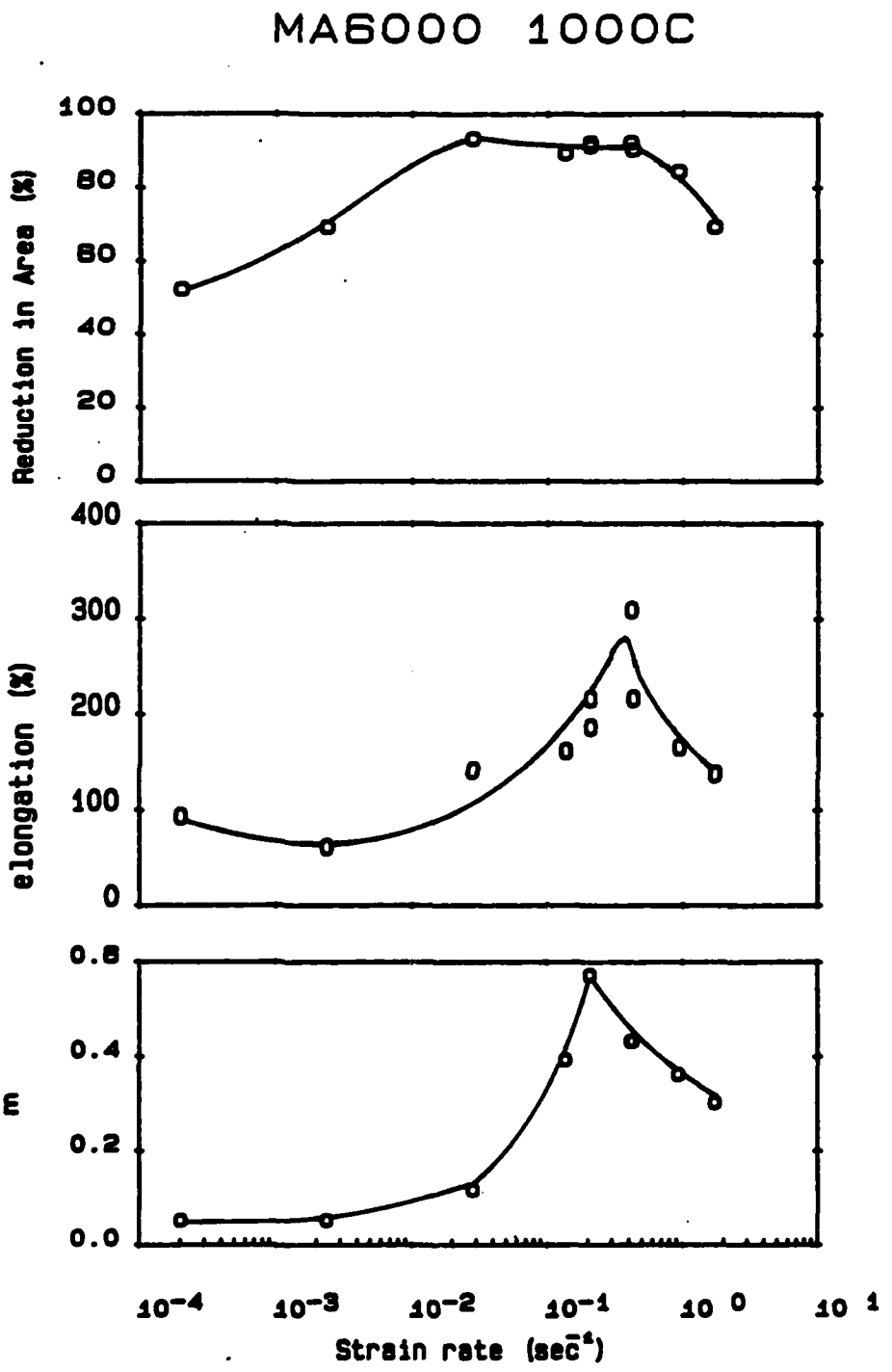

Fig. 6. A comparison of tensile ductility (as indicated by percent reduction of area and percent elongation to failure) with the strain rate sensitivity, m, for different strain rates. As expected, the percent elongation correlates with m.

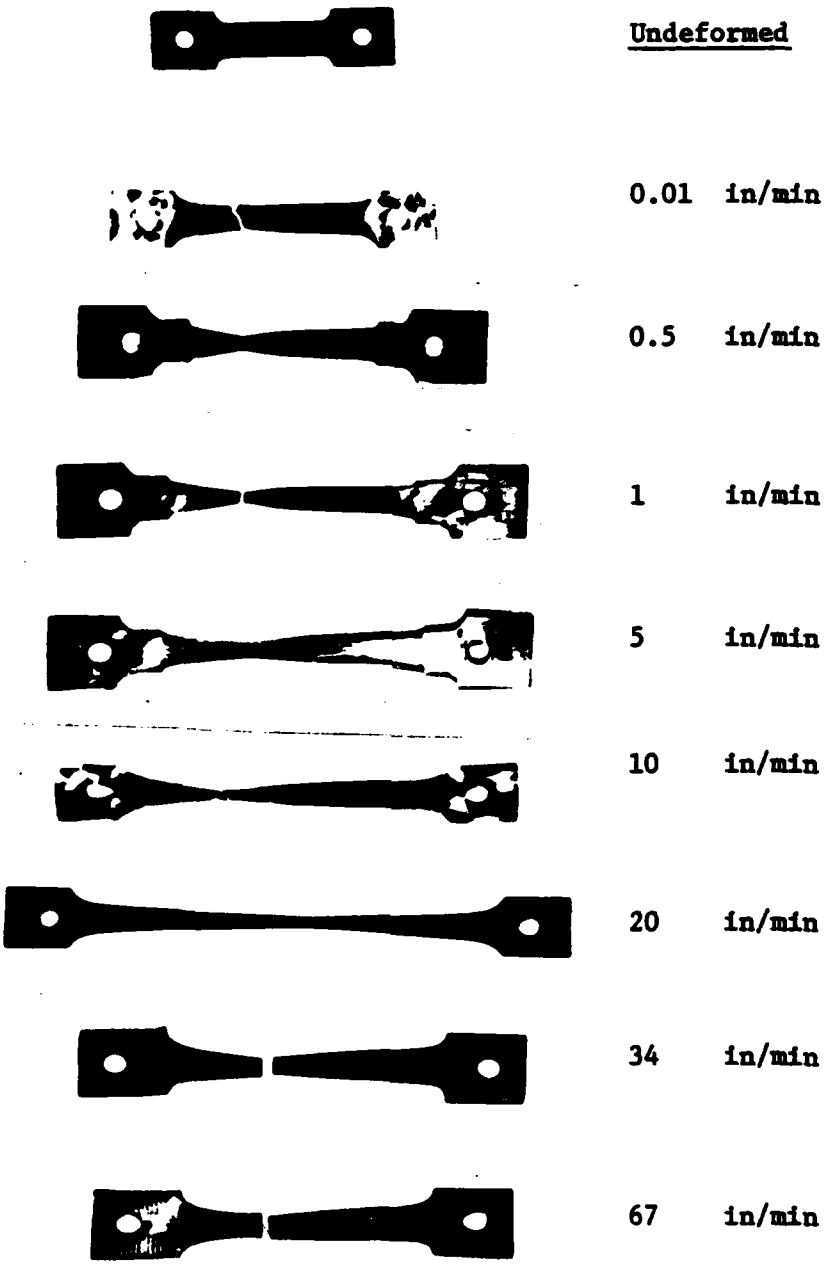

Fig. 7. Appearance of samples of MA 6000 after deformation at various extension rates at 1000 C.

strain rates is by a ductile tearing mode, as opposed to the brittle fracture seen at high strain rates.

More can be learned about the deformation of these materials by examining the microstructures after deformation. MA 754 deformed at 1100 C, 0.01 in/min is shown in Fig. 8. The arrow is parallel to the tensile axis. As compared with Fig. 1, the grain boundaries are much straighter, and regions of very low dislocation density are observed. Thus, there must have been recrystallization. At higher strain rates, there is also evidence for recrystallization as well as grain growth. The micrograph in Fig. 9 shows MA 754 deformed at 1000 C, 2 in/min. A twin is visible at the upper left, and the grain shown is double the initial grain size. Additionally, regions which are free of particles are observed. At very high deformation rates, for example, 900 C, 120 in/min, corresponding to a strain rate of 2.9 s^{-1}, the microstructure is very similar to the as-received structure, as can be seen in Fig. 10. No twins are observed.

Similar phenomena have been noted for MA 6000. At the superplastic strain rate of 0.48 sec^{-1}, obtained at 20 in/min, and 1000 C, some dislocation activity and slight grain elongation may be seen, as shown in Fig. 11. However, at higher strain rates, obtained at 67.2 in/min and 1000 C, for a strain rate of 1.78 s^{-1}, the structure more closely resembles the as-received microstructure. This is demonstrated in Fig. 12.

Conclusions:

1) Strain rates which are most like the strain rates experienced during hot working are approximately 1.5 s^{-1}.
2) Recrystallization and grain growth occur in MA 754 deformed at low and

Fig. 8. TEM micrograph of MA 754 after deformation at 0.01 in/min and 1100 C.

Fig. 9. TEM micrograph of MA 754 after deformation at 2 in/min and 1000 C.

Fig. 10. TEM micrograph of MA 754 after deformation at 120 in/min and 900 C.

Fig. 11. TEM micrograph of MA 6000 after deformation at 20 in/min and 1000 C.

Fig. 12. TEM micrograph of MA 6000 after deformation at 67 in/min and 1000 C.

intermediate strain rates.

3) Cavitation occurs at low strain rates for both alloys.

4) The most likely possibility for deforming fine grained oxide dispersion strengthened superalloys and developing a coarse grained microstructure by annealing will involve deformation at strain rates of at least 1-5 s^{-1} .

B. A Model for Deformation of Fine Grained ODS Alloys Based on The Coupling of Dislocation Creep and Diffusional Deformation

A simple technique for coupling diffusional and dislocation creep mechanisms is used to describe deformation of fine grained polycrystalline solids. The analysis gives a description of the transition from power law creep at high strain rates to diffusional creep at lower strain rates. The analysis also indicates that regions which deform by power law creep gradually disappear as the transition occurs. This behavior bears some resemblance to the "core-mantle" picture of superplastic flow.

The analysis can be used to describe superplastic flow provided the solid is composed of two kinds of grains having different sizes or different physical properties. In this respect the model is patterned after the work of Raj and Ghosh [1,2], who recognized the importance of grain size and physical property distribution effects in superplastic flow. In this approach a distinct mechanism of superplasticity is not required. The regime of high strain rate sensitivity is a natural consequence of the transition from power law creep to diffusional flow in a solid with distributed grain sizes or physical properties. This same view was expressed in a phenomenological way by Hart [3].

In the present treatment we consider the coupling of dislocation creep and diffusional flow in solids containing finely distributed oxide particles. We will assume that the oxide particles can lead to threshold stresses for each of the two creep processes. In the case of dislocation creep, a threshold stress can arise if dislocations are pinned by the particles. If the normal and shear stresses on the particle-matrix interface are fully relaxed, the particles can act like small voids and a critical stress, typically about one half the Orowan stress, is needed to cause dislocation glide. For diffusional creep, particles can inhibit climbing grain boundary dislocations and again a threshold stress can be produced. It seems likely that the threshold stress for diffusion in the grain boundary, σ_o^{gb} , would be smaller than that for dislocation creep, σ_o^{d} .

We start the analysis by considering an array of square grains all having the same size subjected to a pure shear stress, as shown in Fig. 13. The effects of grain size distribution are included in the model but are not discussed here.

Deformation is assumed to occur by diffusional processes near the grain corners (the unshaded areas in Fig. 13) and by dislocation processes far from the corners (the shaded areas). Because different mechanisms of deformation occur in the two regimes, the normal stresses on the boundaries are not uniform, as shown in the figure.

The overall stress and strain rate can be found from the conditions of compatibility and mechanical equilibrium. Compatibility is ensured by requiring the strain rates in the shaded and unshaded areas to be the same. Mechanical equilibrium is satisfied by

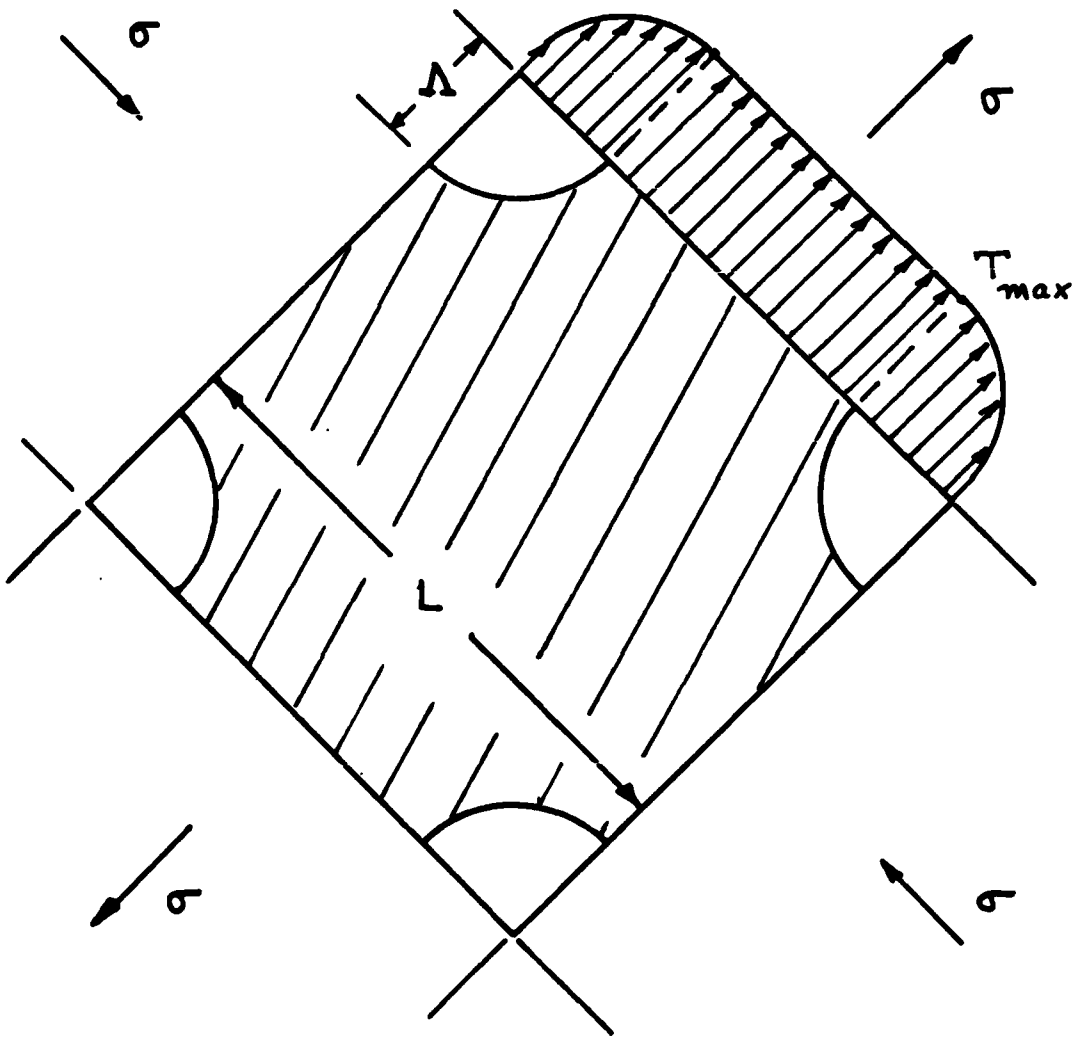

Fig. 13. A square grain model of deformation. Deformation occurs by diffusional flow in the unshaded areas and by dislocation creep in the shaded areas.

$$\sigma L = \int_0^L T_n(x)\, dx \qquad (1)$$

where $T_n(x)$ is the normal stress acting on the boundary at any point, x.

The rate of deformation in the unshaded areas can be described by a modified Coble creep expression of the form

$$\dot{\varepsilon} = \frac{\delta D_{gb} \Omega}{\Lambda^3 kT} (T_{max} - \sigma_o^{gb}) \quad , \qquad (2)$$

where Λ is the diffusion length as shown in Fig. 13, T_{max} is a measure of the stress acting on the boundary and σ_o^{gb} is the critical stress needed to drive diffusional deformation. By invoking the condition of equilibrium the traction T_{max} can be related to the applied stress, σ, and this leads to a diffusional flow equation of the form

$$\dot{\varepsilon} = \frac{8 \delta D_{gb} \Omega}{L^3 kT} \frac{(\sigma - \sigma_o^{gb})}{\alpha^3 (1 - \frac{\alpha}{3})} \qquad (3)$$

where

$$\alpha = \frac{2\Lambda}{L} \qquad (4)$$

is the ratio of the diffusional lengths to the length of the boundary. When $\alpha = 1$ deformation occurs entirely by diffusional processes, whereas when $\alpha < 1$, deformation involves the coupling of diffusional and dislocation creep.

When dislocation creep occurs (in the shaded regions in Fig. 13), the rate of flow there is expressed as

$$\dot{\varepsilon} = A D_L \left(\frac{\mu b}{kT}\right) \left(\frac{T_{max} - \sigma_o^d}{\mu}\right)^n \qquad (5)$$

where σ_o^d is the threshold stress for dislocation creep. In terms of the applied stress (using the condition of mechanical equilibrium) this becomes

$$\dot{\varepsilon} = A D_L \left(\frac{\mu b}{kT}\right) \left[\frac{\sigma - \sigma_o^d + \frac{\alpha}{3}(\sigma_o^d - \sigma_o^{gb})}{\mu (1 - \frac{\alpha}{3})}\right]^n \quad . \qquad (6)$$

Compatibility is ensured by equating the strain rates in equations (3) and

(6). This leads to a solution for α, the parameter that determines the extent of diffusional flow that occurs:

$$\alpha = \left[\frac{8\,\delta\,D_{gb}\,\Omega}{L^3\,kT\,\dot{\epsilon}}\left\{\mu\left[\frac{\dot{\epsilon}}{A D_L}\left(\frac{kT}{\mu b}\right)\right]^{1/n} + \left(\sigma_o^d - \sigma_o^{gb}\right)\right\}\right]^{1/3} . \qquad (7)$$

The flow properties of fine grained solids can then be found by solving equations (3) and (7) simultaneously. Figure 14 shows the kinds of flow properties that can be predicted with this model. We believe it will be possible to rationalize the flow properties given in Figs. 3 and 4 with this new model.

C. High Temperature Creep of Coarse Grained MA 754

Oxide dispersion strengthened (ODS) nickel based superalloys owe their high temperature creep strength to the presence of oxide particles, which inhibit dislocation motion, and to the existence of highly elongated grain structures. At temperatures above 1000 C (0.76 T_m) it appears that the creep performance of these alloys is limited by the degradation of transverse grain boundaries. During the past year substantial progress has been made in investigating the constant stress creep properties of coarse grained MA 754. In addition we have started to characterize the degradation of transverse grain boundaries that occurs during high temperature creep.

1. Creep Testing of MA 754

The constant stress creep properties of MA 754 at elevated temperatures (1000 C - 1300 C) are being measured in vacuum using a creep machine originally built by Lund [4]. As noted in the previous progress report,

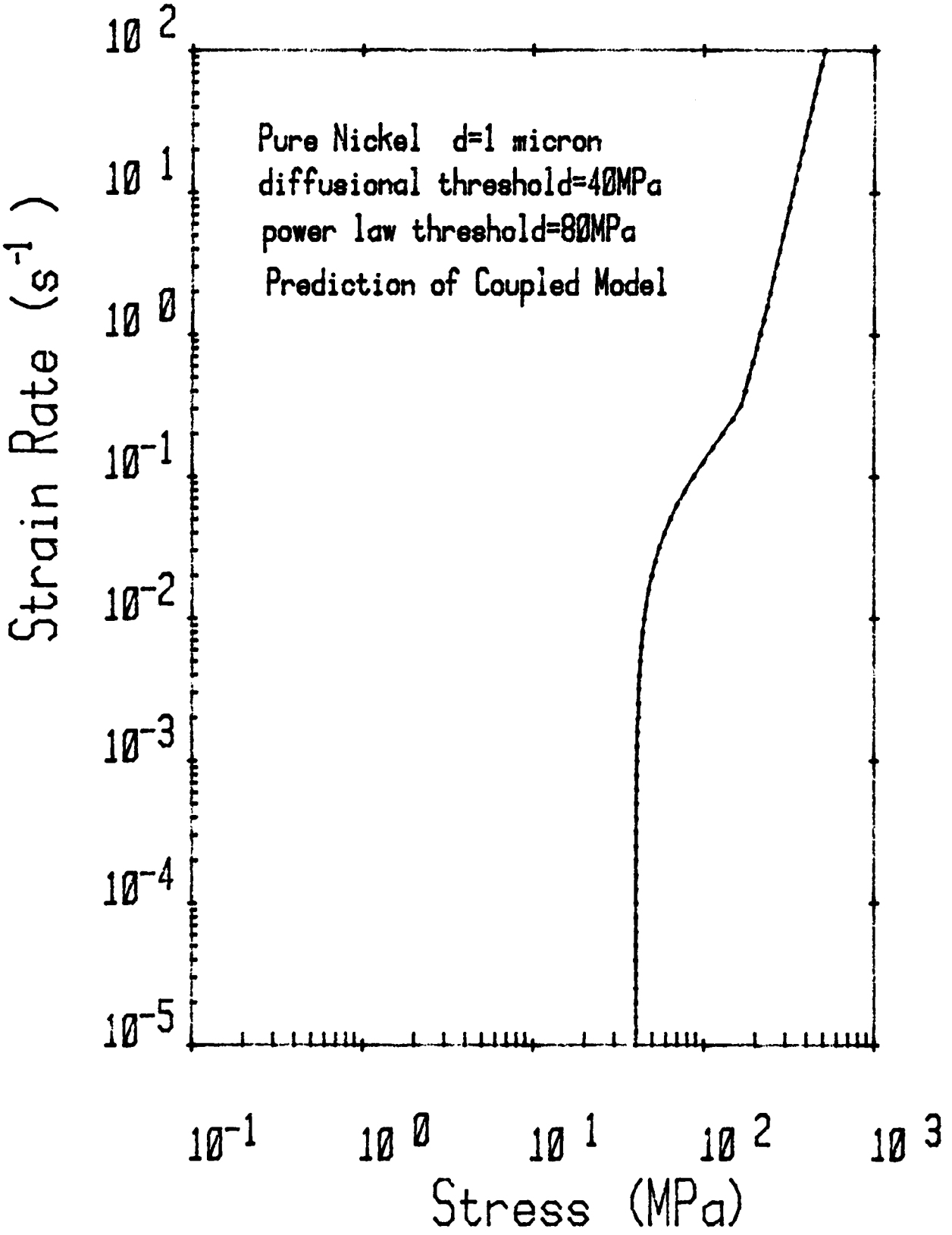

Fig. 14. Model predictions for the steady state flow properties of fine grained ODS nickel at 1000 C.

we have made substantial improvements to this machine to ensure reliability of the entire system and to permit creep testing up to 100 hrs.

All testing of MA 754 to date has been conducted in the longitudinal direction (stress axis parallel to the extrusion direction) in the as received, coarse grained condition. The composition of the ingot being studied (Heat # DT 06A72B2-1) is shown in Table I. Measured steady state strain rates for MA 754 at four temperatures (1000, 1093, 1200 and 1300 C) are shown in Fig. 15 as a function of applied stress. The test data at 1000, 1093 and 1200 C all indicate two distinct regions of deformation, as indicated by the stress exponent n,

$$n = \frac{d \log (\dot{\varepsilon}_{ss})}{d \log (\sigma)} \quad . \tag{8}$$

TABLE I: CHEMICAL COMPOSITION OF MA 754 (HEAT NO. DT06A7B2-1)

Cr	20 wt. %
Fe	1.5 wt. %
Ti	1.0 wt. %
Al	0.6 wt. %
Y_2O_3	0.6 wt. %
Ni	balance

In addition to the above analysis, other ingots have repeatedly shown:

C	0.05 - 0.07 wt. %
O_2	0.33 - 0.40 wt. %
S	0.002 - 0.003 wt. %
N_2	0.12 - 0.13 wt. %

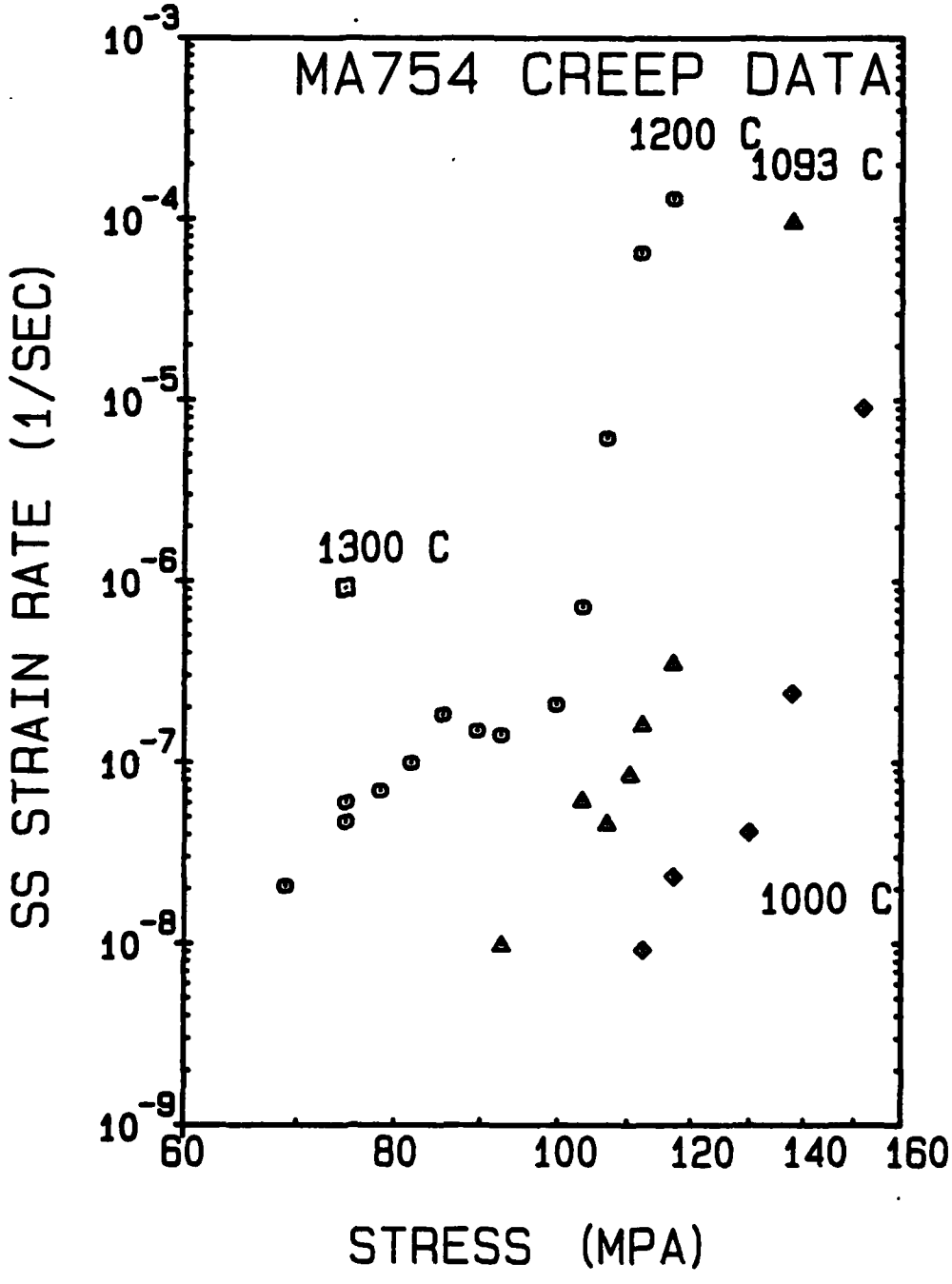

Fig. 15. Steady State Strain Rate as a function of applied stress for MA 754 in the large-grained condition, longitudinal testing direction. Testing performed at temperatures of 1000, 1093, 1200 and 1300 C. Data at 1000, 1093 and 1200 C indicate a low stress exponent regime at the lower stresses, followed by an increase in the stress exponent at higher stresses.

At high applied stresses, n is very high, ranging from 28 at 1000 C and 1093 C to 38 at 1200 C. However, at lower applied stresses a lower value of n, where n ranges from 6.0 to 10.8, is found. The values of n in these two regimes and the transition stresses at the three temperatures are summarized in Table II.

TABLE II: SUMMARY OF MEASURED STRESS EXPONENTS FOR MA 754

Temperature	High Stress Regime	Low Stress Regime	Transition Stress (MPa)
1200 C	38	6	103
1093 C	28	10.8	112
1000 C	28	7.9	135

The deformation behavior of MA 754 in the high stress regime can be explained readily by comparing the high stress exponents with those observed for single crystal TD-Ni-20Cr [4]. At high applied stresses deformation occurs by means of dislocation motion within the grains, and the presence of transverse grain boundaries in the specimen is somewhat unimportant. Hence, the high stress exponents found for polycrystalline MA 754 are similar in magnitude to those measured for single crystals of TD-Ni-20Cr.

At the lower applied stresses, the presence of transverse boundaries becomes quite important. Lower strains to fracture are observed in the low stress regime. The transition in creep behavior also results in a change in the macroscopic appearance of the fractured specimens. This effect is

illustrated in Fig. 16 for specimens tested at 1200 C. At high stresses, the fracture is uniformly slanted across the width of the specimen, indicating that failure occurred transgranularly via shearing of the specimen. As the stress is decreased, the slant fracture disappears, and the fracture appears square, incidating that the fracture has become predominantly intergranular in nature. SEM examination of fracture surfaces indicates that in this low stress regime the elongated grains pull away from each other. Similar cavitation behavior was observed by Howson et al [5] in tests of MA 754 at 1093 C.

It is interesting to compare the 1093 C creep data of Whittenberger [6] and Howson et al [5] with the results of the present investigation. Figure 17 shows the steady state strain rate as a function of stress for all three investigations. It should be noted that the grain aspect ration (GAR) of the material tested in this investigation is higher than that of the previous investigations. As Fig. 17 indicates, the material with a higher GAR seems to require a higher applied stress to reach the same strain rate.

The lowest steady state creep rate measured to data in this investigation has been of the order of $10^{-8}s^{-1}$, as creep strain has been measured by the displacement of the load train outside of the vacuum. Work has commenced on the construction of a tantalum extensometer which will enable us to measure the specimen strain directly in the vacuum. This will enable us to extend our measurements to applied stresses less than or equal to those of previous investigations.

Stress rupture curves for MA 754 at temperatures of 1093 C and 1200 C

MA 754 1200 C FRACTURE

APPLIED STRESS (MPa)

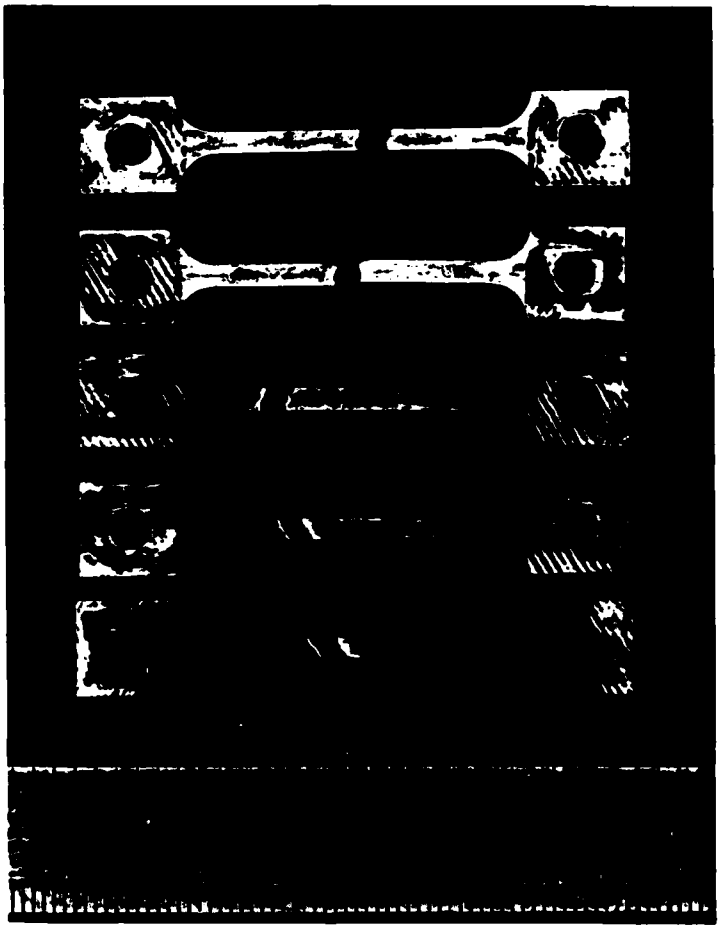

Fig. 16. Macroscopic appearance of 1200 C fractured creep specimens. Slanted fracture appearance of high stress specimens is indicative of transgranular fracture; at lower stresses the overall appearance is square, indicative of predominently intergranular fracture.

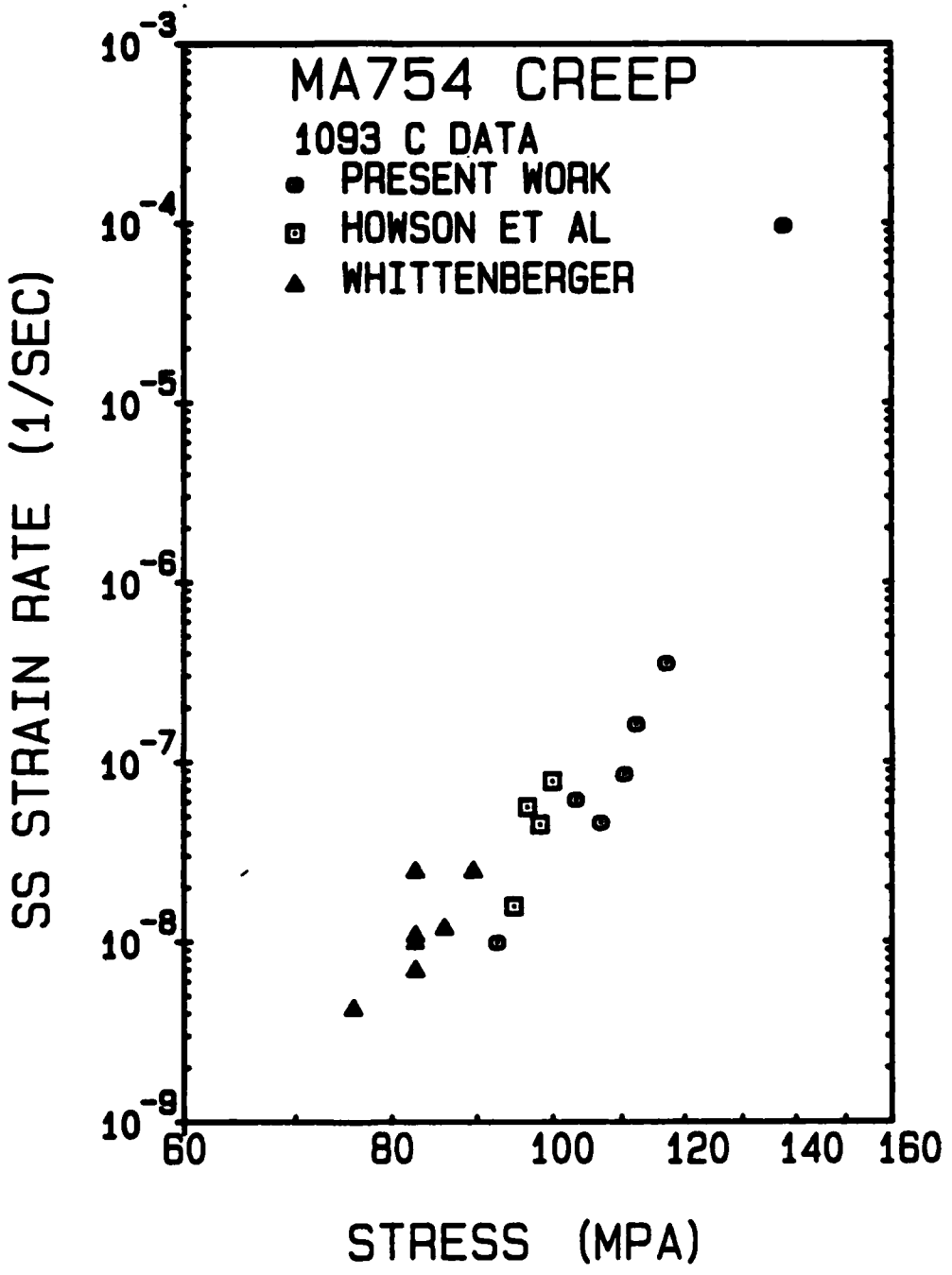

Fig. 17. Steady State Strain Rate as a function of applied stress for MA 754 in the large-grained condition. Longitudinal testing direction. 1093 C data from the present investigation, Howson et al. [5], and Whittenberger [6]. The grain aspect ratio of MA 754 used in this investigation is higher than that of previous investigations.

are shown in Figs. 18 and 19,respectively. By analogy with the strain rate-stress relations, the 1200 C stress-life curve shows different slopes at high and low stresses. It is expected that more tests in the 0.1 to 10 hr range at 1093 C will show the same kind of behavior. That is, at high stresses (short times to rupture) the effect of cavitation of the transverse grain boundaries is negligible, and the stress rupture plots show a characteristically low slope. As the stress decreases (and rupture time increases) the effects of cavitation become significant and the slope of the stress-life curve becomes steeper.

2. Microstructural Evidence for Transverse Grain Boundary Degradation in MA 754

A significant amount of effort has been devoted to indentifying the deformation processes occurring in the transverse grain boundaries of MA 754 specimens tested at low stresses. Cavitation is generally observed in the transverse grain boundaries; it is most concentrated at transverse boundaries one or two grain lengths away from the fracture surface. This indicates that deformation in MA 754 becomes quite localized within the gage section. This is not unexpected, in view of the low strain-rate sensitivity for coarse-grained MA 754.

Previous investigators have reached different conclusions with regard to grain boundary degradation in MA 754. Whittenberger [6] cites optical micrographs as evidence of dispersoid-free zone formation in MA 754. Such evidence (optical micrographs) assumes that the larger oxide inclusions in MA 754 act as markers of diffusional transport (the Y_2O_3 dispersoids cannot be resolved by optical microscopy). On the other hand, Howson et al.

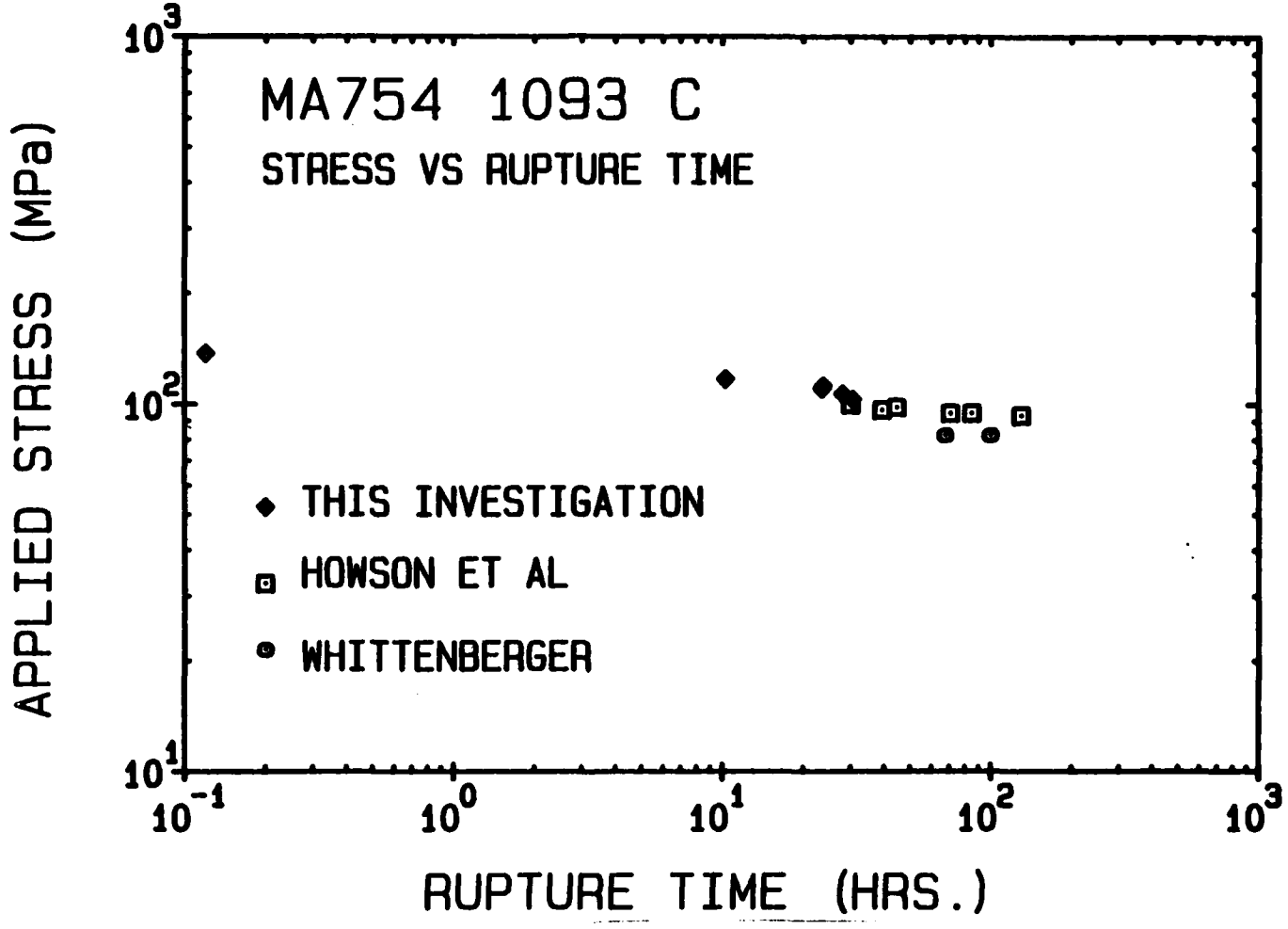

Fig. 18. 1093 C stress rupture data for MA 754. Data from present investigation, Howson et al. [5], and Whittenberger [6]. The slope of the curve appears to increase as lower stresses are considered.

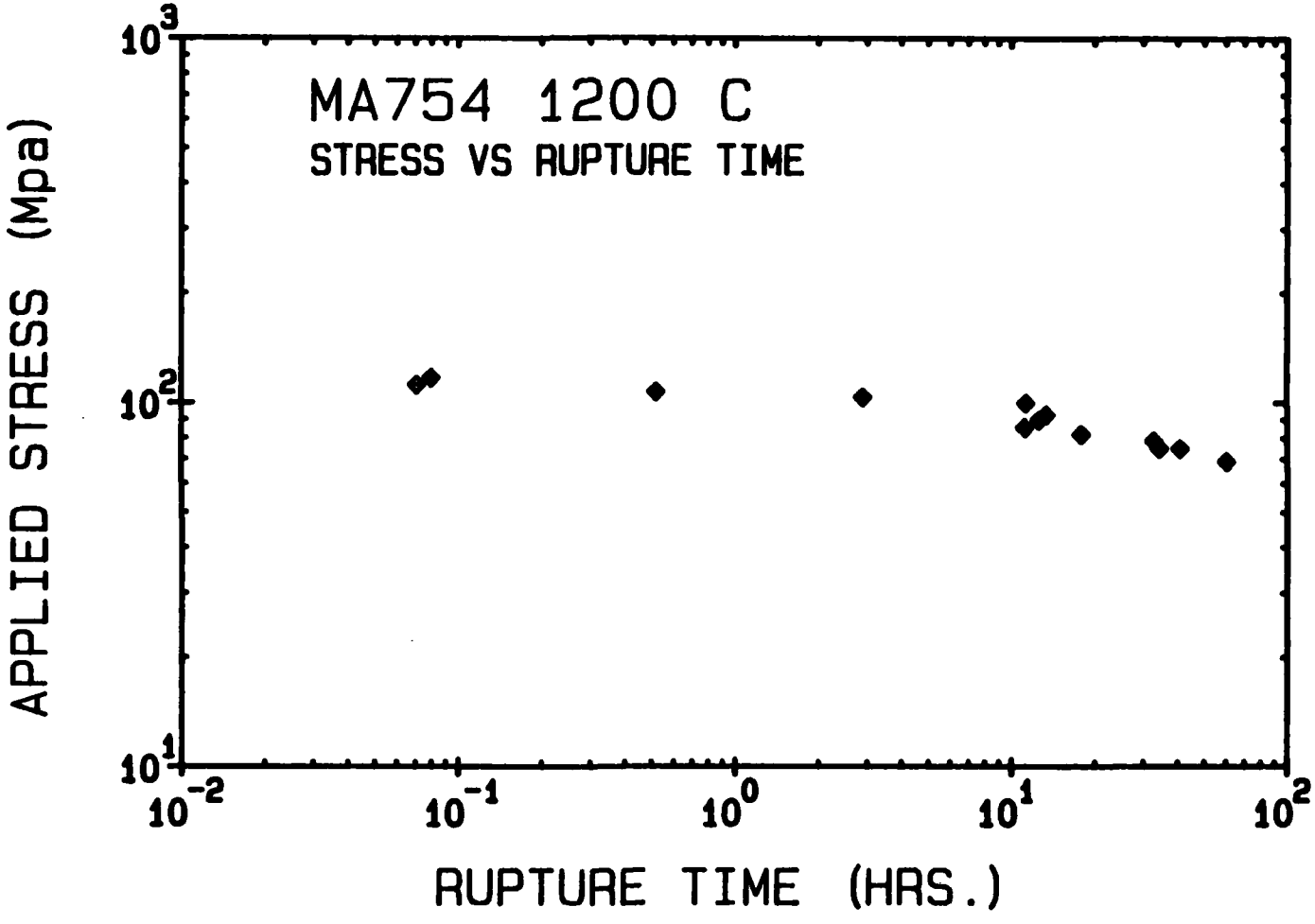

Fig. 19. 1200 C stress rupture data for MA 754. Again, the slope of the stress rupture line is more nearly horizontal at higher stresses, and increases in magnitude as one goes to lower stresses.

[5] failed to find dispersoid-free zones in MA 754 but did observe cavitation on transverse grain boundaries.

Results of the present investigation indicate that small, dispersoid free zones, of the order of one micron in thickness, may form adjacent to cavities on transverse grain boundaries. The most direct evidence has been found by thinning crept specimens for TEM using the window method. Figure 20 is a TEM micrograph of a transverse grain boundary adjacent to a cavity in a specimen crept to failure at 1093 C, 15 ksi (103.4 MPa). It is evident that a small dispersoid-free zone, of the order of one micron in thickness, has formed adjacent to the cavity. This would indicate that short range diffusion of matter occurs from the cavity to the transverse grain boundary, thereby producing a dispersoid free zone next to the grain boundary.

In light of the above results, electron microprobe work was undertaken in order to see if dispersoid-free zones are formed away from cavities in the transverse grain boundaries. An ARL microprobe, operating at 15 kV and with a beam width of one micron, was used to conduct wavelength dispersive analyses for Cr, Ni and Y. The only transverse grain boundary regions which yielded low concentrations of Y, and hence indicated Y_2O_3-free regi were zones immediately next to the cavities. Figures 21 and 22 show regions labeled "A" and "B" which were found to have low Y concentrations. Note that three of the four spots illustrated occur on "islands" between grain boundary cavities. Such islands are presumably where diffusive transport is most intense.

MA 754 103.4 MPa (15.0 ksi), 1093 C

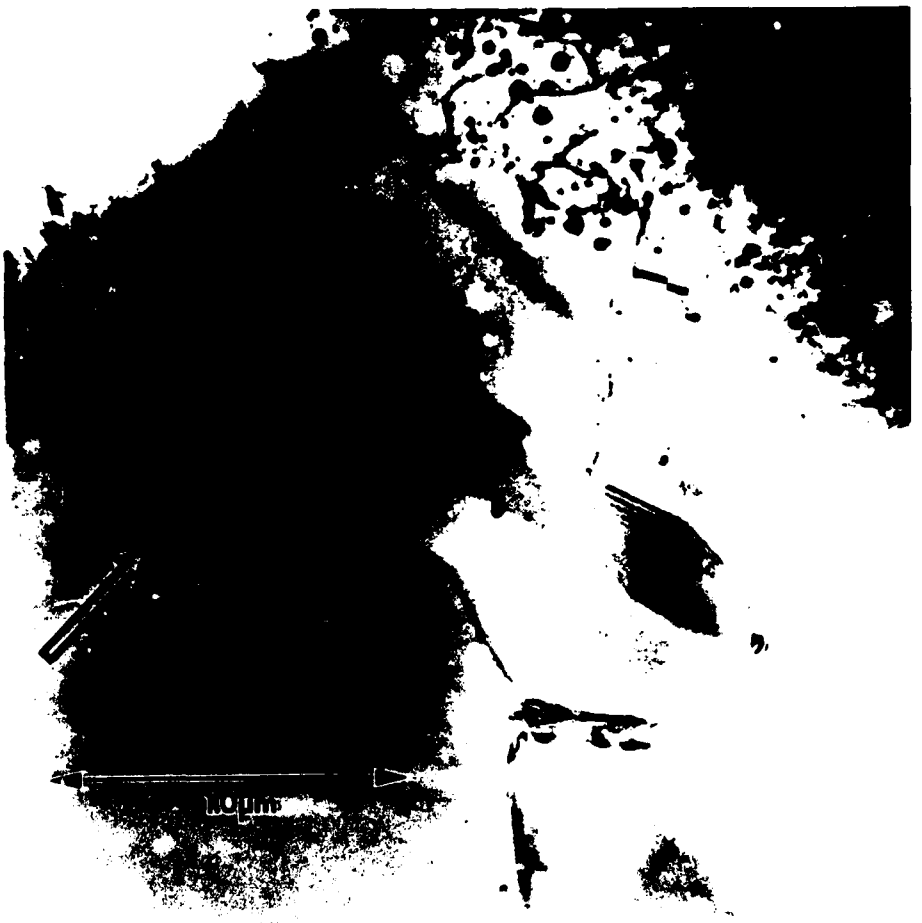

Fig. 20. TEM micrograph of dispersoid free zone in MA 754 adjacent to a transverse grain boundary cavity on the right. Specimen was crept to failure at 103.4 MPa, 1093 C. Black arrow indicates applied stress axis.

MA 754 112.4 MPa (16.3 ksi), 1093 C

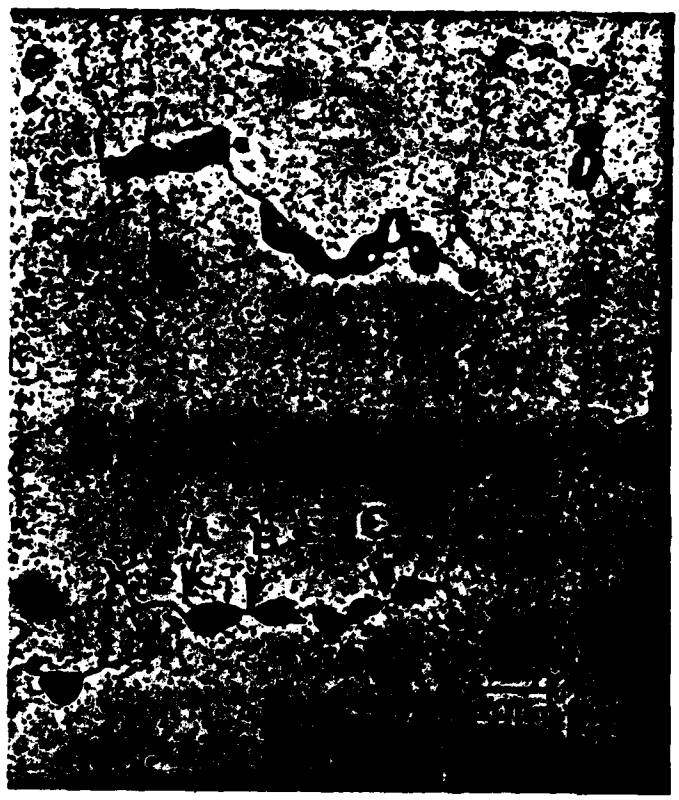

Fig. 21. Optical micrograph of transverse grain boundary in MA 754 specimen crept to failure at 112.4 MPa (16.3 ksi), 1093 C. Stress axis is vertical. Spots A, B and C were analysed for Yttrium content with an electron microprobe analyzer. Spot A: 0.30 wt % Y. Spot B: 0.01 wt % Y. Spot C: 0.01 wt % Y. Interior spot analyses shows average Y content of the alloy (as Y_2O_3) is 0.5 wt %.

MA 754 69.0 MPa (10.0 ksi), 1200 C

Fig. 22. Optical micrograph of transverse grain boundary in MA 754 specimen crept to failure at 69.0 MPa (10.0 ksi), 1200 C. Stress axis is vertical. Spots A and B were analyzed for Yttrium content with an electron microprobe analyser. Spot A: 0.03 wt % Y. Spot B: 0.02 wt % Y. Spot analyses in the grain boundary away from cavities and in grain interiors shows average Y content of the alloy (as Y_2O_3) is 0.5 wt %.

Further TEM and electron microprobe work is needed to more completely characterize the transverse grain boundary structures in crept specimens of MA 754. A new, automated electron microprobe is currently being installed at Stanford, this instrument will allow grid-mapping for Y in the vicinity of cavities on transverse grain boundaries. Observations of the gradients of Y_2O_3 around the cavity should contribute substantially to our understanding of how deformation occurs in the cavitated region.

Extension of creep testing of MA 754 to lower stress will allow us to characterize the onset of cavitation and the corresponding degradation in MA 754. All of the dispersoid-free zones next to cavities have been observed to date in ruptured specimens; it would be interesting to determine that point on the creep curve at which dispersoid free zones adjacent to cavities first appear.

Summary

1. Steady state creep tests on coarse grained MA 754 at high temperatures indicate a high stress exponent for creep at high stresses and a low stress exponent at low stresses.

2. Fracture in the low stress regime is intergranular; at high stresses it is transgranular.

3. Small dispersoid free zones, of the order of one micron in thickness, have been observed adjacent to cavities on transverse grain boundaries. This appears to be a degradation process that results in fracture.

D. Structure and Properties of Al-Fe-Ce Alloys

We are interested in studying the high temperature creep properties of Al-Fe-Ce alloys made by rapid solidification. We believe that the properties of these materials may be similar to those of oxide dispersion strenghthened aluminum alloys. We also believe that high temperature strengths of these materials might be improved by mechanical alloying. Such additional processing would produce very fine oxide and carbide particles within the microstructure and would increase the strength and stability of the microstructure.

Much of our effort during the past year has been devoted to the acquisition of suitable experimental materials. Because rapidly solidified materials fall under "Export Control Regulations" there are limitations in the extent to which we can have access to information about these materials. The presence of foreign nationals (graduate students) in our Department means that such information cannot be freely disseminated or discussed. After several discussions with, and letters to, Mr. Walter Griffith of AFWAL/ML we obtained verbal approval to acquire Al-Fe-Ce alloys for the purpose of research. We have obtained an extrusion of this material through the courtesy of Dr. Sharon Langenback of Lockheed, Burbank. This material will be used in our study of the structure and high temperature creep properties. We have also obtained powder from Mr. Fred Mullen of AFWAL, again after consultation with Mr. Griffith. We plan to mechanically alloy this powder to determine if the structure can be refined and if oxides and carbides can be introduced into the microstructure. These materials have just arrived and we are just starting to characterize their structures.

REFERENCES

1. R. Raj and A. K. Ghosh, Acta Metall., 29, 283 (1981).

2. A. K. Ghosh and R. Raj, Acta Metall., 29, 607 (1981).

3. E. W. Hart, Acta Metall., 15, 1545 (1967).

4. R. W. Lund, Ph.D. Dissertation, Stanford University (1975).

5. T. E. Howson, J. E. Stulga and J. K. Tien, Metall. Trans., 11A, 1599 (1980).

6. J. D. Whittenberger, Metall. Trans., 8A, 1155 (1977).

III. PUBLICATIONS, REPORTS AND DISSERTATIONS RELATING TO THIS AND PREVIOUS AFOSR GRANTS ON OXIDE DISPERSION STRENGTHENED METALS

A. Publications

1. J. H. Holbrook and W. D. Nix, "Edge Dislocation Climb over Non-Deformable Circular Inclusions", Metall. Trans., 5, 1033 (1974).

2. M. Vikram Rao and W. D. Nix, "Creep in Binary Solid Solutions: A Possible Explanation for Anomalous Behavior", Scripta Met., 7, 1255 (1973).

3. M. A. Burke and W. D. Nix, "Plastic Instabilities in Tension Creep", Acta Met., 23, 793 (1975).

4. R. W. Lund and W. D. Nix, "On High Creep Activation Energies for Dispersion Strengthened Metals", Metall. Trans., 6A, 1329 (1975).

5. R. W. Lund and W. D. Nix, "High Temperature Creep of Ni-20Cr-2ThO_2 Single Crystals", Acta Met., 24, 469 (1976).

6. G. M. Pharr and W. D. Nix, "A Comparison of the Orowan Stress with the Threshold Stress for Creep for Ni-20Cr-2ThO_2 Single Crystals", Scripta Met., 10, 1007 (1976).

7. J. H. Hausselt and W. D. Nix, "Dislocation Structure of Ni-20Cr-2ThO_2 After High Temperature Deformation", Acta Met., 25, 595 (1977).

8. J. H. Hausselt and W. D. Nix, "A Model for High Temperature Deformation of Dispersion Strengthened Metals Based on Substructural Observations in Ni-20Cr-2ThO_2", Acta Met., 25, 1491 (1977).

9. R. F. Singer, W. Blum and W. D. Nix, "The Influence of Second Phase Particles on the Free Dislocation Density During Creep of Stainless Steel", Scripta Met., 14, 755 (1980).

10. R. F. Singer, W. C. Oliver and W. D. Nix, "Identification of Dispersoid Phases Created in Aluminum During Mechanical Alloying", Metall. Trans., 11A, 1895 (1980).

11. P. S. Gilman and W. D. Nix, "The Structure and Properties of Al-Al_2O_3 Alloys Produced by Mechanical Alloying:Powder Processing and Resultant Powder Structures",Metall. Trans. 12A, 813 (1981).

12. W. C. Oliver and W. D. Nix, "The Effects of Strain Hardening in the Hydrostatic Extrusion of Axisymmetric Bi-Metal Rods", Metals Technology, February, 75 (1981).

13. W. D. Nix, "The Effects of Grain Shape on Nabarro-Herring and Coble Creep Processes", Metals Forum, 4, 38 (1981).

14. W. C. Oliver and W. D. Nix, "High Temperature Deformation of Oxide Dispersion Strengthened Al and Al-Mg Solid Solutions", Acta Metall., 30, 1335 (1982).

15. D. M. Barnett, W. C. Oliver and W. D. Nix, "The Binding Force Between and Edge Dislocation and a Fermi-Dirac Solute Atmosphere", Acta Metall., 30, 673 (1982).

16. D. M. Barnett, G. Wong and W. D. Nix, "The Binding Force Between a Peierls-Nabarro Edge Dislocation and a Fermi-Dirac Solute Atmosphere", Acta Metall., 30, 2053 (1982).

B. Ph.D. Dissertations

1. R. W. Lund, "A Study of High Temperature Creep of Dispersion Strengthened Ni and Ni-20Cr", Ph.D. Dissertation, Stanford University (1975).

2. J. H. Holbrook, "A Theoretical Investigation of Creep of Dispersion Strengthened Crystals", Ph.D. Dissertation, Stanford University (1976).

3. P. S. Gilman, "The Development of Aluminum-Aluminum Oxide Alloys by Mechanical Alloying", Ph.D. Dissertation, Stanford University (1979).

4. W. C. Oliver, "Strengthening Phases and Deformation Mechanisms in Dispersion Strengthened Solid Solutions and Pure Metals", Ph.D. Dissertation, Stanford University (1981).

C. Oral Presentations (Speaker Underlined)

1. W. D. Nix, "On the Existence of Steady State Creep", Department of Mechanical Engineering, University of Colorado, Boulder, Colorado (December, 1973).

2. W. D. Nix, "Plastic Instabilities in Tension Creep", Air Force Conference on: Fracture and Fatigue of Two Phase Materials - Effects of Plastic Instability, Fairborn, Ohio (September, 1974).

3. W. D. Nix, "High Temperature Creep of Dispersion Hardened Single Crystals", TMS-AIME (invited paper), University of Toronto (May, 1975).

4. W. D. Nix, "When are Back (Threshold) Stresses Meaningful ?" 1977 Gordon Conference on Physical Metallurgy, Holderness School, Plymouth, N. H., June, 1977. (Invited paper).

5. P. S. Gilman and W. D. Nix, "Mechanical Alloying of Al-Al_2O_3 Alloys", presented at 1978 Spring meeting of AIME in Denver.

6. W. C. Oliver, R. F. Singer and W. D. Nix, "Formation and Identification of Particles in Dispersion Strengthened Aluminum", presented at 1980 Spring Meeting of AIME in Las Vegas.

7. W. C. Oliver, "Mechanical Alloying", presented at Department of Materials Science and Engineering, Industrial Affiliates Meeting at Stanford, June, 1980.

8. W. D. Nix, "Creep of Dispersion Strengthened Metals", presented at EXXON Research Laboratory, Linden, N.J., February, 1980.

9. J. K. Gregory, R. Sinclair and W. D. Nix, "Abnormal Grains in MA753", Annual Meeting of AIME, Chicago, February, 1981.

10. J. K. Gregory, J. C. Gibeling and W. D. Nix, "Superplastic Behavior in MA 6000E", International Symposium on Superplastic Forming of Structured Alloys, San Diego, California, June, 1982.

11. J. K. Gregory and W. D. Nix, "A Model for Superplastic Flow Based on the Coupling of Power Law Creep and Diffusional Deformation", International Symposium on Superplastic Forming of Structural Alloys, San Diego, California, June, 1982 (Poster Session).

IV. PROFESSIONAL PERSONNEL

The following personnel of the Department of Materials Science and Engineering at Stanford have been engaged in this research program:

Principal Investigator:

Dr. William D. Nix, Professor

Senior Research Associate:

Dr. Jeffery C. Gibeling

Graduate Research Assistants:

Ms Jean K. Gregory	B.S.	Massachusetts Inst. of Technology
	M.S.	Stanford University
Mr. John J. Stephens	B.S.	Cornell University
	M.S.	Stevens Institute of Technology
Mr. M. Lufti Ovecoglu	B.S.	Middle East Technical University, Ankara
	M.S.	Middle East Technical University, Ankara

11. CONTROLLING OFFICE NAME AND ADDRESS Air Force Office of Scientific Research (NE) Bolling AFB, Building 410 Washington, D.C. 20332	12. REPORT DATE Dec 82 13. NUMBER OF PAGES 26
14. MONITORING AGENCY NAME & ADDRESS *(if different from Controlling Office)*	15. SECURITY CLASS. *(of this report)* UNCLASSIFIED 15a. DECLASSIFICATION/DOWNGRADING SCHEDULE

16. DISTRIBUTION STATEMENT *(of this Report)*

Approved for public release;
distribution unlimited.

17. DISTRIBUTION STATEMENT *(of the abstract entered in Block 20, if different from Report)*

18. SUPPLEMENTARY NOTES

END

FILMED

3-83

DTIC